Article

Capping of the N-terminus of PSD-95 by calmodulin triggers its postsynaptic release

Yonghong Zhang[1,†], Lucas Matt[2,†], Tommaso Patriarchi[2,3,†], Zulfiqar A Malik[2], Dhrubajyoti Chowdhury[2], Deborah K Park[2], Alessandra Renieri[3], James B Ames[1,*] & Johannes W Hell[2,**]

Abstract

Postsynaptic density protein-95 (PSD-95) is a central element of the postsynaptic architecture of glutamatergic synapses. PSD-95 mediates postsynaptic localization of AMPA receptors and NMDA receptors and plays an important role in synaptic plasticity. PSD-95 is released from postsynaptic membranes in response to Ca^{2+} influx via NMDA receptors. Here, we show that Ca^{2+}/calmodulin (CaM) binds at the N-terminus of PSD-95. Our NMR structure reveals that both lobes of CaM collapse onto a helical structure of PSD-95 formed at its N-terminus (residues 1–16). This N-terminal capping of PSD-95 by CaM blocks palmitoylation of C3 and C5, which is required for postsynaptic PSD-95 targeting and the binding of CDKL5, a kinase important for synapse stability. CaM forms extensive hydrophobic contacts with Y12 of PSD-95. The PSD-95 mutant Y12E strongly impairs binding to CaM and Ca^{2+}-induced release of PSD-95 from the postsynaptic membrane in dendritic spines. Our data indicate that CaM binding to PSD-95 serves to block palmitoylation of PSD-95, which in turn promotes Ca^{2+}-induced dissociation of PSD-95 from the postsynaptic membrane.

Introduction

The vast majority of synapses in the brain use glutamate as neurotransmitter (Micheva *et al*, 2010). It activates postsynaptic AMPA-type glutamate receptors (AMPARs) that are precisely juxtaposed to its presynaptic release site. Periods of heightened synaptic activity lead to activation of NMDA-type glutamate receptors (NMDARs). NMDARs mediate Ca^{2+} influx that can permanently increase the postsynaptic strength causing long-term potentiation (LTP; Lisman & Hell, 2008; Nicoll & Roche, 2013), which is most likely the physiological basis of learning and memory (Morris, 2013).

A critical player in postsynaptic AMPAR targeting is PSD-95 (El-Husseini *et al*, 2000, 2002; Elias *et al*, 2006; Schluter *et al*, 2006). PSD-95 consists of three PDZ domains followed by an SH3 domain and a guanylate kinase homology domain (GK). PSD-95 anchors AMPARs at postsynaptic sites by binding with its first and second PDZ domains to the intracellular C-termini of auxiliary subunits known as transmembrane AMPAR regulatory proteins (TARPs), which include stargazin (Stg, γ_2) and its homologs γ_3, γ_4, and γ_8 (Chen *et al*, 2000; Schnell *et al*, 2002; Opazo *et al*, 2010). Furthermore, PSD-95 is palmitoylated at two cysteine residues (C3 and C5) at its N-terminus, which is required for its postsynaptic localization and for postsynaptic targeting of AMPARs (El-Husseini *et al*, 2002). Ca^{2+} influx through NMDARs causes PSD-95 to be temporarily released from postsynaptic membranes (Sturgill *et al*, 2009; Nelson *et al*, 2013). This release seems to reflect an important step for postsynaptic restructuring leading to enlargement of the postsynaptic site and thereby for an increase in postsynaptic AMPARs during LTP (Sturgill *et al*, 2009). Ultimately, PSD-95 augments postsynaptic AMPAR localization upon Ca^{2+} influx during LTP in part due to stimulation of phosphorylation of the C-terminus of Stg/γ_2 upon NMDAR-mediate Ca^2 influx by the Ca^2/calmodulin (CaM)-dependent kinase CaMKII. This phosphorylation fosters membrane detachment of the C-terminus of Stg/γ_2 and thereby binding of the very C-terminus of Stg/γ_2 to PSD-95 (Tomita *et al*, 2005; Sumioka *et al*, 2010). The initial mobilization of PSD-95 upon Ca^2 influx could either be necessary for structural plasticity to occur or constitute a negative feedback mechanism to curb potentiation.

Ca^{2+}/CaM interacts with PSD-95 and its homologs SAP97 and SAP102 in a Ca^2-dependent manner (Masuko *et al*, 1999; Paarmann *et al*, 2002; Fukunaga *et al*, 2005) and stimulates PSD-95 binding to the non-receptor tyrosine kinase Pyk2 to augment NMDAR activity and thereby LTP (Bartos *et al*, 2010). Previous studies focused on

1 Department of Chemistry, University of California, Davis, CA, USA
2 Department of Pharmacology, University of California, Davis, CA, USA
3 Department of Medical Genetics, University of Siena, Siena, Italy
  *Corresponding author. Tel: +1 530 752 6358; Fax: +1 530 752 8995; E-mail: jbames@ucdavis.edu
  **Corresponding author. Tel: +1 530 752 6540; Fax: +1 530 752 7710; E-mail: jwhell@ucdavis.edu
  †These authors contributed equally

the HOOK region at the C-terminal end of the SH3 domain of PSD-95, SAP97, and SAP102 as the CaM-binding site. We now report that Ca^{2+}/CaM binds not only to the SH3 domain but also to the N-terminal region of PSD-95 as well as the second PDZ domain (PDZ2, residues 155–249). We present the NMR structure of Ca^{2+}/CaM bound to the N-terminal region of a PSD-95 fragment [residues 1–71, called PSD-95(1–71)]. Both CaM lobes collapse around an N-terminal helix of PSD-95 (residues 1–16) and seques-ter two palmitoylation sites (C3 and C5) that mediate postsynaptic targeting of PSD-95. CaM forms extensive contacts with Y12 in PSD-95, and mutating Y12 to Glu prevents binding of CaM to PSD-95 upon Ca^{2+} influx. Importantly, although this mutation does not affect PSD-95 palmitoylation under basal conditions, it counteracts the reduction in palmitoylation of PSD-95 following Ca^{2+} influx and the Ca^{2+}-induced release of PSD-95 from postsynaptic membranes. It also blocks displacement of CDKL5, which binds to the N-terminus of palmitoylated PSD-95 (Zhu *et al*, 2013) and can strengthen postsynaptic responses (Ricciardi *et al*, 2012; Zhu *et al*, 2013). Our results identify the N-terminal CaM-binding site of PSD-95 as a critical regulator of the dynamic postsynaptic localization of PSD-95 and thereby of postsynaptic plasticity.

Results

CaM binds to the N-terminus of PSD-95

To characterize binding of CaM to PSD-95 beyond the established interaction between CaM and the SH3 domain of PSD-95, pull-down assays of CaM were performed with the various GST-tagged PSD-95 fragments (Fig 1A). Accordingly, Ca^{2+}/CaM interacted with the N-terminal region of PSD-95 (residues 1–71 preceding PDZ1), PDZ2, and SH3 but not PDZ3, GK, or GST alone (Fig 1B and D). All samples contained comparable amounts of the respective full-length fusion protein with little to no degradation (Fig 1C). To define the CaM-binding site at the PSD-95 N-terminus more precisely, CaM binding to fluorescein-labeled peptides of residues 1–13, 15–36, 37–52, and 49–65 was monitored by fluorescence polarization (FP; Fig 2A and B). FP of the peptide spanning the first 13 residues showed saturable binding upon adding increasing amounts of CaM. Accordingly, this peptide binds to CaM with a dissociation constant of 18 ± 0.3 μM (Fig 2B, black circles). None of the other peptides (collectively covering residues 15–65) bound CaM at protein concen-trations up to 100 μM (Fig 2B). These results indicate that CaM exhibits Ca^{2+}-induced binding to the first 13 residues of PSD-95.

CaM forms a collapsed structure around the N-terminal helix in PSD-95

NMR spectroscopy was used to characterize the structural interac-tion of CaM bound to PSD-95(1–71). The ^{15}N-^{1}H HSQC NMR spec-trum of ^{15}N-labeled PSD-95(1–71) in the absence of CaM exhibits poor chemical shift dispersion, indicative of an unstructured and random coil conformation (Fig 3A). The NMR assignments for PSD-95(1–71) were determined as shown in Fig 3A. The addition of saturating CaM causes the PSD-95 NMR peaks assigned to residues 1–16 to broaden significantly, whereas the NMR peaks assigned to residues 17–71 were unaffected by CaM. Thus, the CaM-binding site
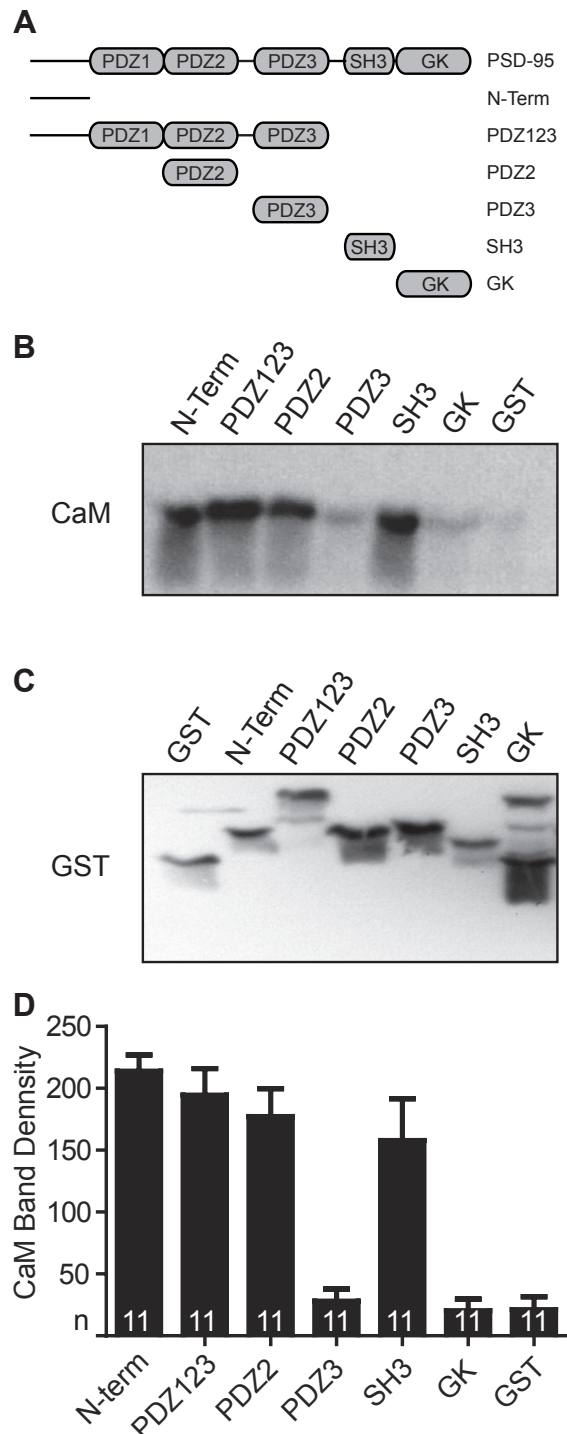

Figure 1. Ca^{2+}/calmodulin (CaM) binds to the N-terminus, PDZ2, and SH3 of PSD-95.

A   Schematic diagram of PSD-95 domains depicting the N-terminal region (residues 1–64), PDZ1–3, SH3, and GK.

B   Pull-down of Ca^{2+}-bound CaM with the various PSD-95 domains.

C   Probing for GST to visualize fusion proteins on a blot run in parallel to the pull-down blot.

D   Relative band intensities from (B) are shown for each PSD-95 domain as determined by densitometry from 11 independent experiments.
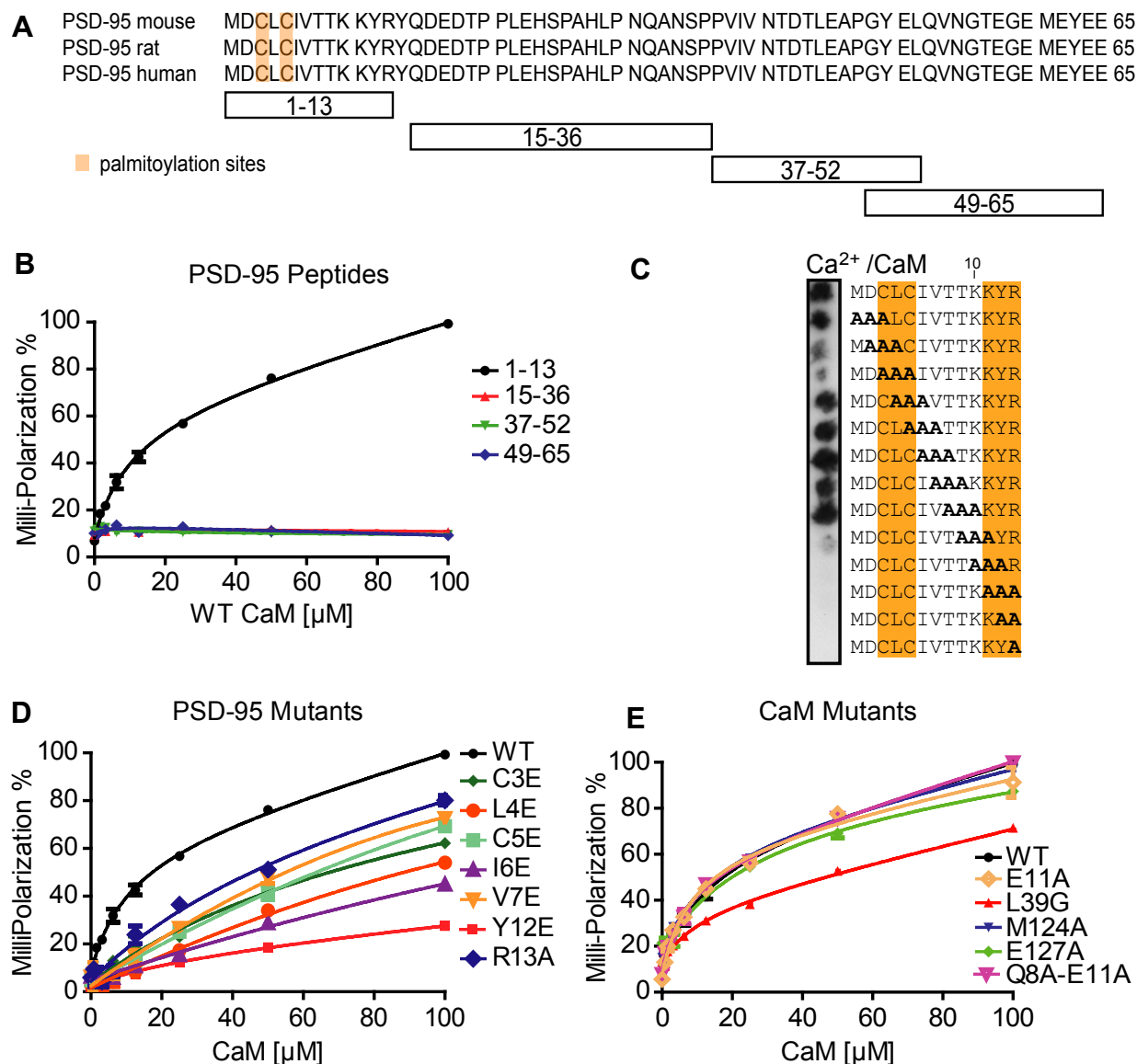
Figure 2. N-terminal 13 residues of PSD-95 bind to Ca^{2+}/CaM.

A   Amino acid sequence of the N-terminal 65 residues of PSD-95. Rectangular boxes underneath define the length of synthetic peptide fragments used in binding assays with Ca^{2+}/CaM. Palmitoylation sites are highlighted in orange.

B   Fluorescence polarization (FP; see Materials and Methods) from each synthetic peptide covalently labeled with fluorescein is plotted as a function of CaM concentration. The increase in FP from the N-terminal peptide (residues 1–13) as a function of increasing CaM concentration indicates binding. The K_d for binding of Ca^{2+}/CaM to the N-terminal peptide is calculated to be 18 μM. None of the other peptides showed any increase in FP as a function of increasing CaM concentration (up to 100 μM), indicating that these peptides do not bind to Ca^{2+}/CaM.

C   Peptide alanine scanning spot array of N-terminal PSD-95 peptide (residues 1–13) for Ca^{2+}/CaM binding. Mutagenesis of PSD-95 residues highlighted in orange show the largest effect on CaM binding.

D   Ca^{2+}/CaM binding to mutant N-terminal PSD-95 peptides (residues 1–13; WT titration is same as in B).

E   Binding of CaM mutants to N-terminal PSD-95 peptide (residues 1–13; WT titration is same as in B).

on PSD-95(1–71) is localized within the first 16 residues from the N-terminus, consistent with the results in Fig 2.

The ^{15}N-^{1}H HSQC NMR spectrum of ^{15}N-labeled Ca^{2+}-free CaM does not change upon adding a 10-fold excess of PSD-95(1–71) (not shown), consistent with a lack of PSD-95 binding to apo-CaM. By contrast, the ^{15}N-^{1}H HSQC NMR spectrum of ^{15}N-labeled Ca^{2+}/CaM changes significantly upon adding a stochiometric amount of

PSD-95(1–71) (Fig 3B). The spectral changes saturate after adding one equivalent of PSD-95(1–71), indicating a 1:1 binding stoichiometry. CaM residues in the N- and C-lobe exhibit amide NMR peaks that either broaden or change chemical shift upon adding PSD-95 (1–71) (Supplementary Table S1), suggesting the respective CaM residues are at or near the PSD-95(1–71) binding site. Most of these residues are clustered in exposed hydrophobic patches on both CaM
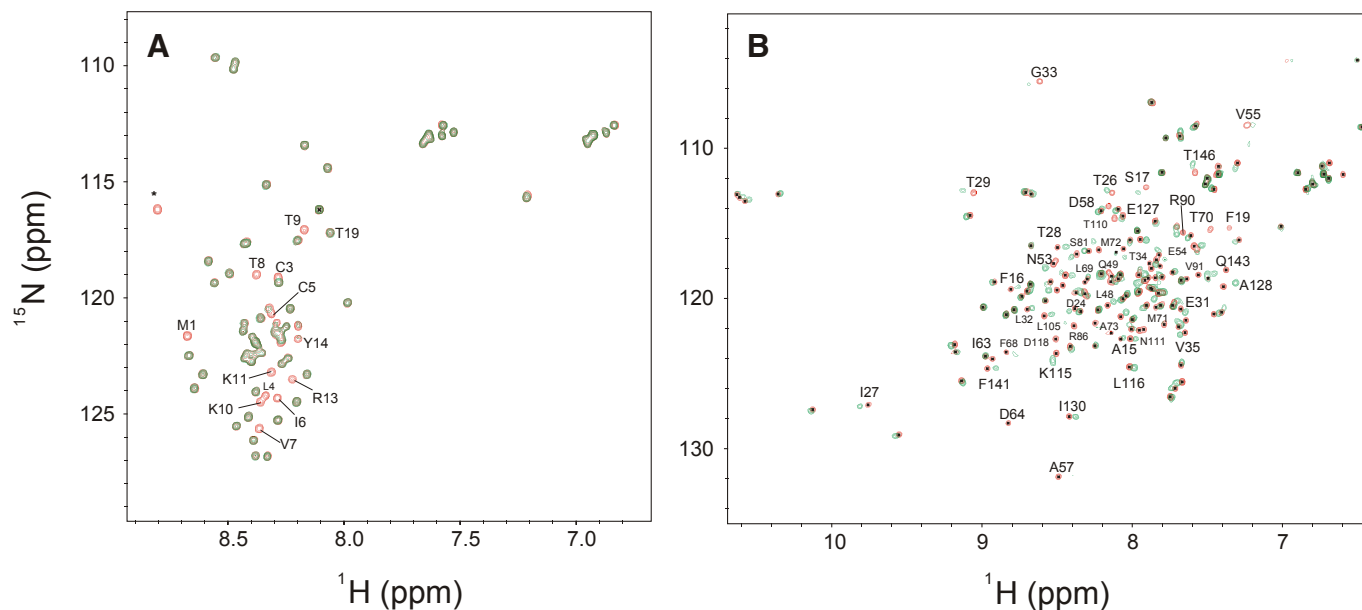
Figure 3. NMR analysis of Ca^{2+}/CaM binding to PSD-95 (1–71).

A   Two-dimensional ^{15}N-^{1}H HSQC spectra of ^{15}N-labeled PSD-95(1–71) in the absence (red) and presence (green) of unlabeled Ca^{2+}/CaM. The NMR resonances assigned to the N-terminal 16 residues in PSD-95 show as much as 100-fold decrease in peak height caused by CaM binding. The NMR assignments have been deposited in the BMRB (Accession Number 19238). The decreased NMR intensity is mostly due to chemical shift exchange broadening at these sites caused by CaM binding that has exchange kinetics on the chemical shift time scale. NMR signals assigned to PSD-95 residues 17–71 are unaffected by CaM binding. NMR resonance assigned to non-native residue (S0) upstream of the N-terminal Met is marked by an asterisk.

B ^{15}N-^{1}H HSQC spectra of ^{15}N-labeled Ca^{2+}/CaM in the absence (red) and presence (green) of unlabeled PSD-95(1–71). CaM residues that show the largest spectral changes caused by binding to PSD-95(1–71) are indicated by residue labels and are listed in Supplementary Table S1.

lobes. However, some CaM residues have NMR signals that are not affected by PSD-95(1–71), including residues in the EF-hand Ca^{2+}-binding loops (G25, G61, G98, G134) and polar surface of the CaM lobes (E7, K13, K30, E114). The lack of chemical shift changes to these residues suggests that the internal main chain structure within each lobe does not change much upon binding to PSD-95(1–71) and target binding is localized mainly to the exposed hydrophobic sites on both CaM lobes.

A detailed protocol for determining the NMR structure of the CaM/PSD-95(1–71) complex is summarized in Supplementary Methods. Residual dipolar couplings (RDCs, Supplementary Fig S1 and Table S2; Tjandra & Bax, 1997) and chemical shift perturbation data (Supplementary Table S1) provided structural restraints for a molecular docking calculation using the software HADDOCK (de Vries *et al*, 2010). Ten lowest energy structures of the CaM/PSD-95 complex are superimposed in Fig 4A and have a main chain RMSD of 0.69 Å (structural statistics in Table 1). The energy-minimized average main chain structure is shown in Fig 4B.

The NMR-derived structure of the CaM/PSD-95(1–71) complex reveals that both lobes of CaM collapse around the N-terminal helix of PSD-95 (residues 1–16) (Fig 4B). The helical structure of the first 16 residues of PSD-95 in the complex was confirmed by circular dichroism (Supplementary Fig S2). Several hydrophobic residues in PSD-95 including L4, I6, V7, and Y12 interact with exposed hydrophobic residues of CaM (Fig 4C and D). Most striking are the two palmitoylation sites (C3 and C5; El-Husseini *et al*, 2002, 2000) in PSD-95 that are completely sequestered by hydrophobic residues in the N-lobe of CaM (F19, L32 and L39). Also noteworthy is that

PSD-95 Y12 fits into a cavity formed by CaM residues in the C-lobe (M124, E127, V136, F141, and M144). In addition to hydrophobic contacts, PSD-95 K10 forms a salt bridge with CaM E11, which might play a role in specifying the orientation of the PSD-95 helix bound to CaM, and PSD-95 R13 forms salt bridges with E114 and E120 of CaM. The two lobes of CaM in the complex form interdomain contacts between L39 and V108 (Fig 4B, N-lobe: pink and C-lobe: red), which stabilize a collapsed structure of CaM as seen in previous structures of CaM bound to various target proteins (Hoeflich & Ikura, 2002). The EF-hand interhelical angles for CaM bound to PSD-95 are typical for Ca^{2+}-bound EF-hands in the familiar open conformation (87° from EF1, 106° for EF2, 91° for EF3 and 97° for EF4).

Our structural model of CaM bound to the PSD-95 N-terminus reveals that the two palmitoylation sites in PSD-95 (C3 and C5) are almost completely buried by CaM and therefore not accessible. To test whether CaM blocks the accessibility of C3 and C5, we monitored whether CaM can inhibit the covalent attachment of a fluorescent dye (fluorescein-5-maleimide) at both C3 and C5 in PSD-95 (1–71). This modification should mimic the attachment of palmitate at these sites. Fluorescein-5-maleimide is a thiol-reactive molecular probe that should specifically attach to both C3 and C5 in PSD-95 (1–71). The dye was added to PSD-95(1–71) with no CaM, Ca^{2+}/CaM, or apo-CaM. After removing unreacted dye, fluorescence emission spectra were recorded for each sample (Supplementary Fig S3A). Fluorescence was 50% less following incubation in the presence of Ca^{2+}/CaM compared with no CaM or apo-CaM. These results indicate that Ca^{2+}/CaM decreases the efficiency with which
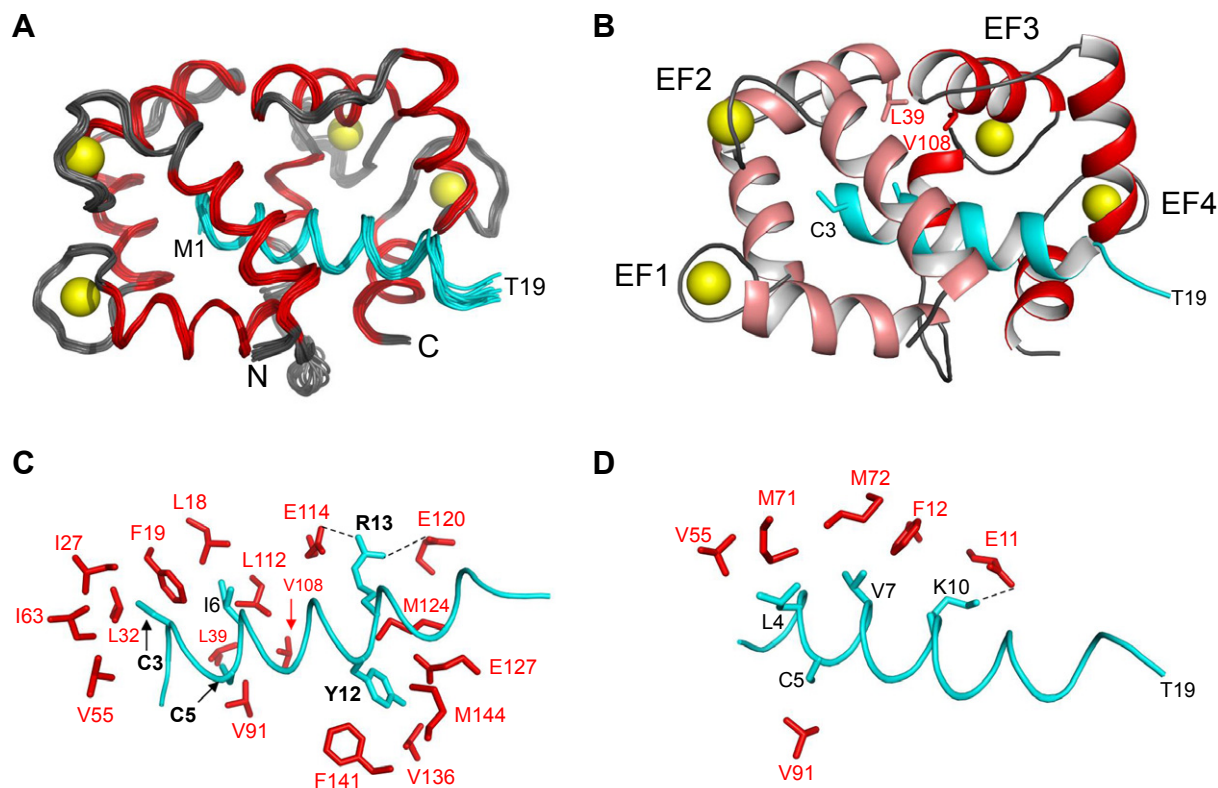
Figure 4. Ca^{2+}/CaM forms a collapsed structure around the N-terminal helix of PSD-95.

A   Superposition of main chain atoms of 10 lowest energy NMR-derived structures of CaM (red) bound to the N-terminal helix in PSD-95 (cyan). Bound Ca^{2+} is depicted in yellow. The atomic coordinates have been deposited into the Protein Databank (2MES).

B   Ribbon representation of the energy-minimized average main chain structure of CaM (N-lobe: pink, C-lobe: red) bound to the N-terminal helix of PSD-95 (cyan). The four EF-hands in CaM are labeled EF1, EF2, EF3, and EF4. Side-chain atoms of CaM residues (L39 and V108) show contact between N-lobe (pink) and C-lobe (red).

C, D   Close-up view of exposed side-chain atoms in CaM (red) interacting with side-chain atoms from PSD-95 residues C3, C5, I6, Y12 and R13 (C) or L4, V7 and K10 (D). Salt bridges to PSD-95 K10 and R13 are depicted by dashed lines.

the fluorescein dye is attached to PSD-95 likely by blocking the accessibility of the two cysteines. PSD-95 will spend some fraction of time free of CaM even in the presence of stoichiometric amounts of Ca^{2+}/CaM, which would allow fluorescein attachment of PSD-95 to build up over time and could explain partial rather than full block of fluorescein attachment.

To further demonstrate that Ca^{2+}/CaM binding and palmitoylation of C3 and C5 in PSD-95 are mutually exclusive, we examined whether the attachment of fluorescein at C3 and C5 might prevent binding of Ca^{2+}/CaM. Indeed, the ^{15}N-^1H HSQC NMR spectrum of ^{15}N-labeled CaM does not substantially change upon adding a stoichiometric amount of fluorescein-labeled PSD-95(1–71) (Supplementary Fig S3B) in contrast to the dramatic change upon addition of a stoichiometric amount of unconjugated PSD-95(1–71) (Fig 3B). These results show that Ca^{2+}/CaM binds preferentially to unconjugated PSD-95(1–71), consistent with binding of Ca^{2+}/CaM to depalmitoylated but not palmitoylated PSD-95.

Mutagenesis of CaM/PSD-95 structural interface weakens binding

To validate the NMR structural model of the CaM/PSD-95 complex, Ala scanning was performed through the peptide that covers the

first 13 N-terminal residues of PSD-95. Peptides were spot synthesized on a membrane and probed by overlay with Ca^{2+}/CaM, which was detected with an anti-CaM antibody (Fig 2C). Substitution of PSD-95 residues Y12 and R13 by Ala either individually or combined completely abolished binding to CaM in this assay, consistent with these residues making multiple contacts with CaM as seen in our structure (Fig 4C and D). Substitution of L4 with Ala also decreased the binding affinity to CaM at least when combined with two additional Ala substitutions (Fig 2C), consistent with L4 making hydrophobic contacts with CaM (Fig 4D). However, triple Ala mutations of C5, I6 and V7 that form contacts with CaM did not substantially affect CaM binding (Fig 2C), perhaps because Ala is similar enough to these residues to retain binding. Instead of using Ala mutations, the PSD-95 residues (C3, C5, I6 and V7) were replaced with the more polar Glu for more quantitative analysis by FP. As expected, all of the Glu mutants (C3E, L4E, C5E, I6E and V7E) weaken CaM binding to PSD-95 (Fig 2D; Supplementary Table S3), consistent with each of these residues making hydrophobic contacts with CaM (Fig 4C and D).

The CaM/PSD-95 structure was further validated by mutations in CaM. Mutagenesis of CaM residue L39 to Gly at the lobe interface (L39G) weakens binding to PSD-95 (Fig 2F; Supplementary Table S4). L39 in the CaM N-lobe forms hydrophobic contacts with

Table 1. Structure statistics for NMR-derived structures of Ca^{2+}/calmodulin (CaM)/PSD9$^{5-NT\ complex}$

Parameter	Value
NMR restraints	
Short-range NOEs	12
Dihedral angles	46
Hydrogen bonds	34
Ambiguous interaction restraints (AIR)	69
$^1D_{HN}$ RDC	78
RDC Q-factor[a]	0.11
Ramachandran plot	
Most favored region (%)	86.3
Allowed region (%)	13.7
Disallowed region (%)	0.0
RMSD from average structure (Å)	
CaM backbone atoms	0.59
PSD95 (1–19) backbone atoms	0.70
All backbone atoms	0.69

[a]Q-factor = RMS($D^{calc} - D^{obs}$)/RMS(D^{obs}), where D^{calc} and D^{obs} are calculated and observed residual dipolar couplings (RDC) values, respectively.

V108 from the C-lobe that stabilizes interaction between the two lobes in the collapsed CaM/PSD-95 structure (Fig 4B). The L39G mutation abolishes the hydrophobic interaction with V108, which weakens contact between the two lobes and destabilizes the collapsing of the two lobes around the N-terminus of PSD-95. Thus, a cooperative interaction of both CaM lobes is necessary to create proper binding to PSD-95 and explains why residues from both the N-lobe and C-lobe participate in binding to PSD-95 (Fig 4C and D). The cooperativity of the lobes is also consistent with the observation that the individual CaM lobes (N-lobe: residues 1–77 and C-lobe: residues 82–148), which are structured (Zhang *et al*, 2012), cause no detectable change in the NMR spectrum of PSD-95(1–71) (Supplementary Fig S4), in contrast to the large spectral change induced by full-length CaM.

PSD-95 residue Y12 forms extensive contacts with CaM (Fig 4C). The Y12E mutation disrupts hydrophobic interactions with CaM residues (M124, V136, F141, M144) and weakens the binding affinity by approximately 37-fold (Fig 2D; Supplementary Table S3). In addition to the hydrophobic contacts, the phenolic side chain of Y12 forms a hydrogen bond with the side-chain carboxyl group of CaM residue E127. The E127A mutation in CaM eliminates this hydrogen bond and weakens the binding affinity by 2.5-fold (Fig 2E; Supplementary Table S4), which in terms of free energy is consistent with the loss of a hydrogen bond, further confirming the CaM/PSD-95 structure.

N-terminal Ca^{2+}/CaM binding impairs PSD-95 palmitoylation and CDKL5 binding

To test in intact cells whether Ca^{2+} influx negatively controls palmitoylation of PSD-95, HEK293 cells were transfected with PSD-95^{WT} and PSD-95^{Y12E}. Y12 makes multiple contacts with Ca^{2+}/CaM, and

changing it to Glu strongly impairs binding of Ca^{2+}/CaM (Fig 2D and E). At the same time, this mutation should not affect basal palmitoylation of PSD-95 *per se*, because Y12 is not located in the palmitoyltransferase binding site (PSD-95 residues 3–9; El-Husseini *et al*, 2000; Fukata *et al*, 2004).

Under basal conditions, PSD-95^{WT} and PSD-95^{Y12E} showed comparable levels of palmitoylation in HEK293 cells (Fig 5A and B). Normal basal PSD-95^{Y12E} palmitoylation is also indicated by clustering of the ectopically expressed PSD-95^{WT} and PSD-95^{Y12E} when expressed in COS cells (Supplementary Fig S5), which requires palmitoylation (Hsueh & Sheng, 1999; El-Husseini *et al*, 2002; Fukata *et al*, 2013). Ca^{2+} influx mediated by the Ca^{2+} ionophore ionomycin induced a strong loss of palmitoylation of PSD-95^{WT} but not PSD-95^{Y12E} (Fig 5A), indicating that binding of Ca^{2+}/CaM to the N-terminus of PSD-95 shifts PSD-95 toward its depalmitoylated state.

The cyclin-dependent protein kinase-like kinase CDKL5 binds to the first 19 residues of PSD-95 but only if PSD-95 is palmitoylated (Zhu *et al*, 2013). Because postsynaptic targeting of CDKL5 by this interaction augments postsynaptic strength (Zhu *et al*, 2013; see also Ricciardi *et al*, 2012), a functionally important question is whether this interaction is downregulated by Ca^{2+}/CaM. HEK293 cells were co-transfected with PSD-95 and CDKL5 before treatment with ionomycin and co-immunoprecipitation of CDKL5 with PSD-95. As expected from its negative effect on palmitoylation, ionomycin disrupted the co-precipitation of CDKL5 with WT PSD-95 nearly completely (Fig 5C–E). This effect depended on Ca^{2+}/CaM binding to PSD-95 as PSD-95^{Y12E} did not show any loss of co-precipitation upon Ca^{2+} influx and the CaM antagonist calmidazolium (CMZ) prevented the Ca^{2+}-induced loss of co-precipitation of WT PSD-95.

To test whether Ca^{2+}/CaM affects PSD-95 palmitoylation in intact neurons, acute forebrain slices were treated with 100 μM NMDA for 5 min. This treatment triggers postsynaptic Ca^{2+} influx that stimulates recruitment of CaMKII to NMDARs and subsequent phosphorylation of the AMPAR GluA1 subunit on S831 (Leonard *et al*, 1999 #551; Halt *et al*, 2012 #550). Postsynaptic Ca^{2+} influx had been shown earlier to reduce PSD-95 palmitoylation (El-Husseini *et al*, 2002). Accordingly, NMDA treatment reduced PSD-95 palmitoylation (Fig 6A and B). This effect is selective for palmitoylation of PSD-95 as palmitoylation of Gαi3 was unaffected (Fig 6A). NMDA induced in parallel association of Ca^{2+}/CaM with PSD-95 and displacement of CDKL5 from PSD-95 (Fig 6C–E). Importantly, three different CaM antagonists [CMZ, trifluoperazine (TFP), W7] prevented the loss of palmitoylation and of CDKL5 co-precipitation and the increase in CaM co-precipitation. We conclude that NMDAR-mediated Ca^{2+} influx induces CaM binding to PSD-95, thereby reducing both, palmitoylation of PSD-95 and CDKL5 displacement in neurons.

Ca^{2+} influx stimulates loss of WT but not Y12E PSD-95 from spines

Diffusion of PSD-95 out of spines is limited under basal conditions (~15% over 30 min; Steiner *et al*, 2008). Ca^{2+} influx increases the rate of this diffusion of PSD-95 by 2–3-fold (Steiner *et al*, 2008; Sturgill *et al*, 2009; Nelson *et al*, 2013). This activity-triggered increase in PSD-95 mobility is important for LTP (Steiner *et al*,
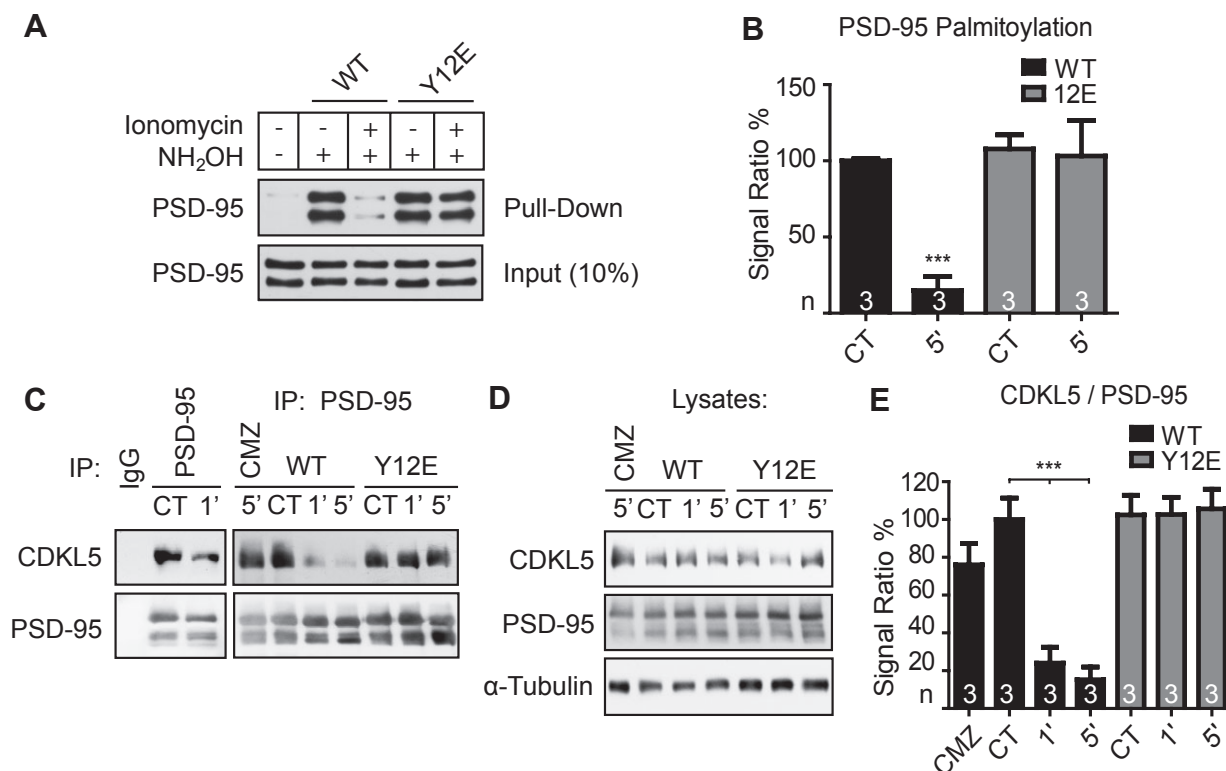
Figure 5. Ca^{2+}/CaM antagonizes palmitoylation of PSD-95 and CDKL5 binding in HEK293 cells.

A, B HEK293T cells were transfected with RFP-PSD-95^{WT} or RFP-PSD-95^{Y12E}. After 24 h, cells were treated with vehicle (CT) or 5 μM ionomycin for 5 min and extracted. NEM was added to alkylate free SH groups on Cys. Palmitoylated Cys were deacylated with hydroxylamine (NH$_2$OH), and newly available SH groups biotinylated for pull-down with streptavidin, followed by immunoblotting for PSD-95. Omission of NH$_2$OH prevented pull-down (left lane) indicating the specificity of this procedure. Ionomycin-induced Ca^{2+} influx decreased palmitoylation of PSD-95^{WT} but not PSD-95^{Y12E}. Total levels of PSD-95^{WT} and PSD-95^{Y12E} were comparable as determined just before pull-down (Input).

C–E HEK293T cells were transfected with RFP-PSD-95^{WT} or RFP-PSD-95^{Y12E} plus CDKL5 for treatment as above, immunoprecipitation of PSD-95, and immunoblotting as indicated. Ionomycin-induced Ca^{2+} influx nearly abolished co-immunoprecipitation of CDKL5 with PSD-95^{WT} but not PSD-95^{Y12E} (C, E). Pre-treatment with CMZ (10 min, 30 μM) prevented loss of CDKL5 co-immunoprecipitation. Lack of PSD-95 and CDKL5 immunoprecipitation by control IgG shows specificity of their co-precipitation (C, left lane). Total expression of PSD-95^{WT} and PSD-95^{Y12E} and of CDKL5 in the various conditions was comparable (D; tubulin served as a loading control). Quantification (E) shows the ratio of CDKL5 co-precipitation versus PSD-95 content in each sample.

Data information: In (B) and (E), data are given as means ± s.e.m., ***P < 0.001, one-way ANOVA with Dunnett's post-test.

2008) and LTD (Nelson *et al*, 2013). Postsynaptic PSD-95 localization requires palmitoylation of C3 and C5 (El-Husseini *et al*, 2000, 2002; Sturgill *et al*, 2009; Fukata *et al*, 2013). Thus, we hypothesized that Ca^{2+} triggered binding of CaM to the very N-terminus of PSD-95, and the consequent shift toward depalmitoy-lated PSD-95 is a major factor in the Ca^{2+}-induced destabilization of postsynaptic PSD-95 localization. We expressed PSD-95^{WT} and PSD-95^{Y12E} with a RFP tag at the C-terminus in cultures of dissociated hippocampal neurons. Brief treatment with glutamate to stimulate Ca^{2+} influx via NMDARs triggered a reduction in the spine-to-shaft ratio for RFP-PSD-95 by about 20% over a 15-min washout period (Fig 7). This reduction reflected a decrease in PSD-95 concentration as it was normalized to changes in spine volume, which was determined by the spine-to-shaft ratio of GFP. Strikingly, PSD-95^{Y12E} not only showed no such reduction, it actually exhibited a remarkably strong increase after 5 and 15 min of glutamate treatment. Again, this increase reflects an increase in concentration as it was normalized to changes in spine size (which were minimal; Fig 7D). We

conclude that CaM binding the N-terminus of PSD-95 curbs its post-synaptic accumulation upon Ca^{2+} influx.

Discussion

PSD-95 possesses multiple CaM-binding sites

By taking a fresh look at CaM binding to PSD-95, we found that Ca^{2+}/CaM specifically binds not only to the previously described HOOK domain but also to the N-terminus (residues 1–16) and to PDZ2 (Fig 1). The existence of several CaM-binding sites within a protein is not unusual. For instance, the central, pore-forming $\alpha_1 1.2$ subunit of the L-type Ca^{2+} channel Ca$_v$1.2 interacts with CaM at its N-terminus and three independent sites near the C-terminus to control fast Ca^{2+}-dependent inactivation of Ca$_v$1.2 (Pitt *et al*, 2001; Dick *et al*, 2008; Evans *et al*, 2011; see also Johny *et al*, 2013) as well as its surface removal via displacement of
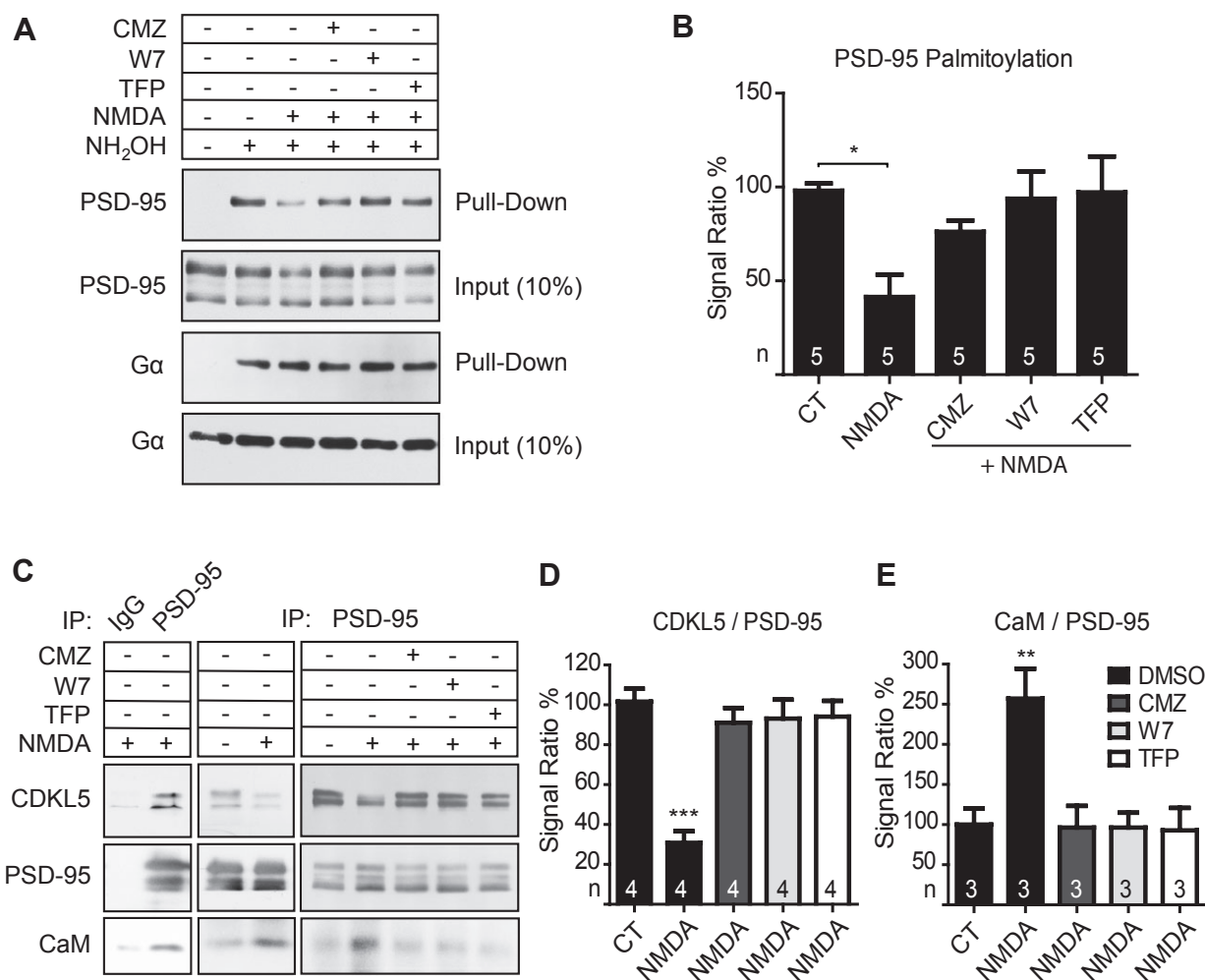
Figure 6. Ca^{2+}/CaM antagonizes palmitoylation of PSD-95 and CDKL5 binding in neurons.

Acute forebrain slices were treated with vehicle (CT) or 100 μM NMDA for 5 min before lysis.

A, B NMDA-induced Ca^{2+} influx decreased palmitoylation of PSD-95 (reduced pull-down by Streptavidin after biotin switch) without affecting total PSD-95 levels (A, C, middle blots). This decrease was blocked by pre-treatment with the CaM antagonists calmidazolium (CMZ; 30 μM), W7 (20 μM), and trifluoperazine (TFP; 20 μM). Note that palmitoylation of the trimeric G protein subunit Gαi3 was not affected by Ca^{2+} influx showing specificity of the effect on PSD-95 and serving as an additional internal loading control.

C–E Co-immunoprecipitation of CaM with PSD-95 was increased and of CDKL5 decreased upon NMDA-induced Ca^{2+} influx. Both effects were blocked by pre-treatment with CMZ, W7, and TFP. Quantification shows ratio of CDKL5 and CaM co-precipitation versus PSD-95 content in each precipitation.

Data information: In (B), (D) and (E) data are given as means ± s.e.m., *$P < 0.05$, **$P < 0.01$, ***$P < 0.001$, one-way ANOVA with Dunnett's post-test.

α-actinin (Hall *et al*, 2013). Ca^{2+}/CaM binding to the HOOK region likely affects interactions of PSD-95 with other binding partners such as the NMDARs (Fukunaga *et al*, 2005; but see Masuko *et al*, 1999), SAP102 (Masuko *et al*, 1999), or Pyk2 (Bartos *et al*, 2010). A potential function of the newly described association of Ca^{2+}/CaM with PDZ2 on similar or other protein interactions is intriguing and will stimulate future work. Here, we focus on the structural and functional analysis of Ca^{2+}/CaM binding to the N-terminus of PSD-95 because this region and specifically its palmitoylation is critical for postsynaptic targeting of PSD-95 and with it of AMPARs (Chen *et al*, 2000; El-Husseini *et al*, 2000, 2002; Schnell *et al*, 2002; Fukata *et al*, 2013).

CaM-binding motif at the PSD-95 N-terminus

The CaM-binding site at the N-terminus of PSD-95 (Figs 1 and 2) differs from other CaM target sites (Hoeflich & Ikura, 2002). It does not follow the consensus sequence of other CaM-binding motifs (IQ, 1–10, 1–14 and 1–16) (Rhoads & Friedberg, 1997). However, PSD-95 N-terminal residues 2–16 have some similarity to the CaM-binding site found in Ca^{2+}/CaM-dependent kinase, CaMKK (residues 338–354, 50% homology and 25% identical; Kurokawa *et al*, 2001). The CaMKK sequence contains an aromatic (F352) and adjacent basic residue (R351), which both form contacts with CaM residues in the C-lobe. The PSD-95 sequence has an aromatic residue (Y14)

preceded by R13 that both form contacts with CaM residues in the C-lobe (E114, E120, M124, E127, V136, F141, M144). The CaMKK sequence also has a conserved leucine (L340) flanked by mostly hydrophobic residues (T339, I341, L342, V343) that each form contacts with CaM residues in the N-lobe. The corresponding residues in the PSD-95 sequence (C3, L4, C5, I6, V7) also form contacts with CaM residues in the N-lobe (L18, F19, I27, L32, L39, V55, I63). The structure of CaM bound to PSD-95 has an inter-lobe contact (between L39 and V108) that is also found in the structure of CaM bound to CaMKK but not in CaM bound to other target proteins (Ikura, 1996; Hoeflich & Ikura, 2002). An important structural difference between CaM/PSD-95 and CaM/CaMKK is that PSD-95 lacks the hairpin-loop structure formed by CaMKK residues (352 – 357), which might explain why CaMKK binds CaM with 10-fold higher affinity than PSD-95.

CaM controls palmitoylation and CDKL5 binding of PSD-95

Palmitoylation–depalmitoylation cycles are highly dynamic and can occur within seconds (Vartak *et al*, 2014). Any interference with palmitoylation is expected to shift this equilibrium toward depalmitoylated protein. Our data show that Ca^{2+} influx into HEK293 cells reduces palmitoylation of PSD-95^{WT} within 5 min by approximately 80% and, based on loss of CDKL5 coprecipitation, this decrease apparently occurs within 1 min (Fig 5). Loss of Ca^{2+}/CaM binding to PSD-95^{Y12E} completely prevents this shift toward depalmitoylation even over the extended 5-min time period. Similarly, Ca^{2+} influx through the NMDAR decreases palmitoylation of endogenous PSD-95 in acute forebrain slices (Fig 6). This decrease is blocked by three structurally very different CaM antagonists again implicating Ca^{2+}/CaM in antagonizing PSD-95 palmitoylation in neurons (Fig 6). We conclude that Ca^{2+}/CaM binding to PSD-95 makes C3 and C5 inaccessible for palmitoyl transferase. Ca^{2+}/CaM might physically block the binding of palmitoyl transferase to PSD-95 at residues 3–9 (El-Husseini *et al*, 2000; Fukata *et al*, 2004). In this manner, Ca^{2+}/CaM shifts the dynamic equilibrium of the constitutive palmitoylation/depalmitoylation cycle toward the latter (Fig 8).

At the same time, Ca^{2+} influx causes a loss of CDKL5 binding to PSD-95 in HEK293 cells (Fig 5) and in neurons (Fig 6). The CDKL5 displacement is of functional interest because CDKL5 has recently been identified as a positive regulator of postsynaptic strength (Ricciardi *et al*, 2012), which depends on CDKL5 binding to the N-terminus of PSD-95 (Zhu *et al*, 2013). Remarkably, this interaction requires palmitoylation of PSD-95 (Zhu *et al*, 2013). It is thus likely that Ca^{2+}/CaM displaces CDKL5 by impairing palmitoylation. In addition, Ca^{2+}/CaM could also directly compete with CDKL5 for binding to PSD-95 in the Y12-T19 region as T19 is critical for CDKL5 binding to a peptide spanning PSD-95 residues 1–19 (Zhu *et al*, 2013).

CaM controls postsynaptic localization of PSD-95

Earlier work indicates that postsynaptic Ca^{2+} influx destabilizes PSD-95 in spines such that a substantially larger fraction (30–50%) than under non-stimulated conditions (15%) of spine PSD-95 exchanges with shaft PSD-95 over a period of 30 min (Steiner *et al*, 2008; Nelson *et al*, 2013). Consistently, postsynaptic Ca^{2+} influx

induces a temporary reduction in total PSD-95 content in spines in our cultures (Fig 7). The loss of PSD-95 is prevented and even over-compensated by our PSD-95^{Y12E} mutant (Fig 7). Collectively, our data indicate that N-terminal capping of PSD-95 by Ca^{2+}/CaM blocks the accessibility of palmitoylation sites at C3 and C5 (Supplementary Fig S3), which prevents palmitoylation of PSD-95 and triggers its redistribution away from postsynaptic membranes at high Ca^{2+} levels (Fig 7). PSD-95 at the postsynaptic membrane is in dynamic equilibrium with palmitoylated and depalmitoylated forms controlled by the relative activity of palmitoyl transferase and esterases (Fukata *et al*, 2004, 2013). In our model (Fig 8), we suggest that palmitoylation of PSD-95 (and hence membrane anchoring) and CDKL5 binding (Zhu *et al*, 2013) are both favored under resting basal conditions (absence of glutamate) when cytosolic Ca^{2+} levels are low. Stimulation of glutamate receptors leads to channel opening that causes Ca^{2+} influx at glutamatergic synapses. The rise in postsynaptic Ca^{2+} level then induces Ca^{2+}/CaM to bind preferentially to depalmitoylated PSD-95 at the N-terminus to promote diffusion of PSD-95 away from the postsynaptic membrane. The Y12E mutation blocks Ca^{2+}/CaM binding to PSD-95 without affecting palmitoylation of PSD-95 because Y12 is located outside the consensus sequence for palmitoylation (El-Husseini *et al*, 2000; Fukata *et al*, 2004). Consistent with our model (Fig 8), PSD-95^{Y12E} prevents Ca^{2+}-induced dissociation of PSD-95 from both CDKL5 (Figs 5 and 6) and its removal from postsynaptic sites (Fig 7). We posit CaM capping of the PSD-95 N-terminus as an important mechanism for decreasing the abundance of PSD-95 and its binding partners at the postsynaptic site in response to Ca^{2+} influx associated with LTD.

Materials and Methods

Ethical approval

All animal procedures had been approved by the University of California at Davis and followed NIH guidelines.

Fluorescence polarization assays

Fluorescein-labeled peptides (100 nM; ChinaPeptides, Shanghai, China) were titrated with increasing concentrations of purified CaM in FP buffer (50 mM HEPES, pH 7.4, 100 mM KCl, 1 mM MgCl$_2$, 10 mM CaCl$_2$, 0.05 mM EGTA, 5 mM nitrilotriacetic acid) and FP determined with a Synergy 2 plate reader (BioTek, Winooski, VT, USA) as described (Lim *et al*, 2002).

Brain slices

Three hundred fifty-micrometer-thick forebrain slices containing hippocampus were prepared from 8- to 14-week-old mice in ice-cold artificial cerebrospinal fluid (ACSF, containing: 127 mM NaCl, 26 mM NaHCO$_3$, 1.2 mM KH$_2$PO$_4$, 1.9 mM KCl, 2.2 mM CaCl$_2$, 1 mM MgSO$_4$ and 10 mM D-glucose, 290–300 mOsm/kg) with a vibratome (Leica VT 1000A) as in Halt *et al*, 2012 and Hall *et al*, 2013. CaM antagonists were applied for 30 min before NMDA (100 μM, 5 min). Slices were frozen and later homogenized in Lysis Buffer (1% Triton X-100, 150 mM NaCl, 10 mM EDTA, 10 mM
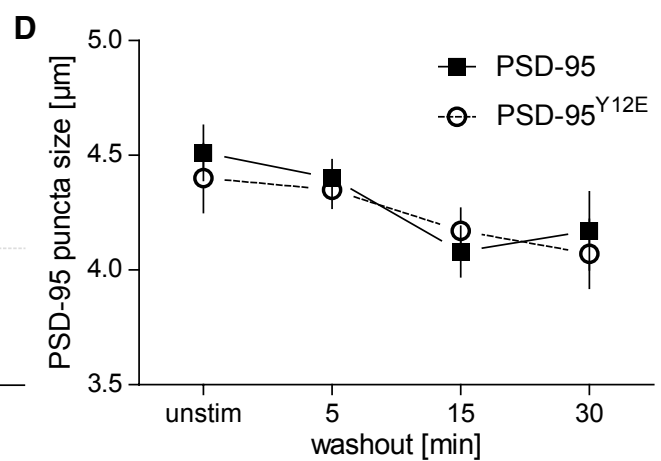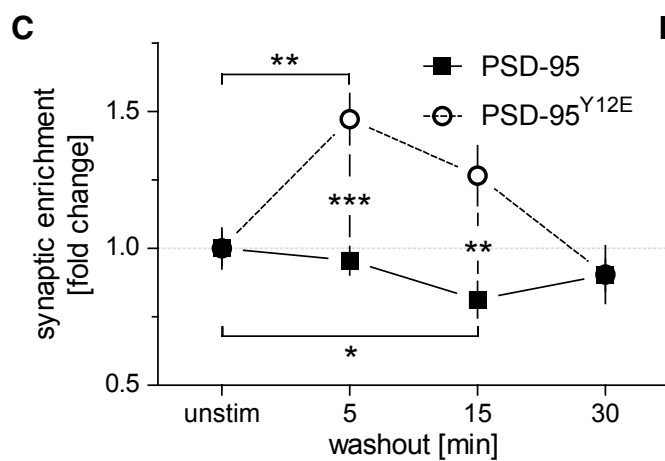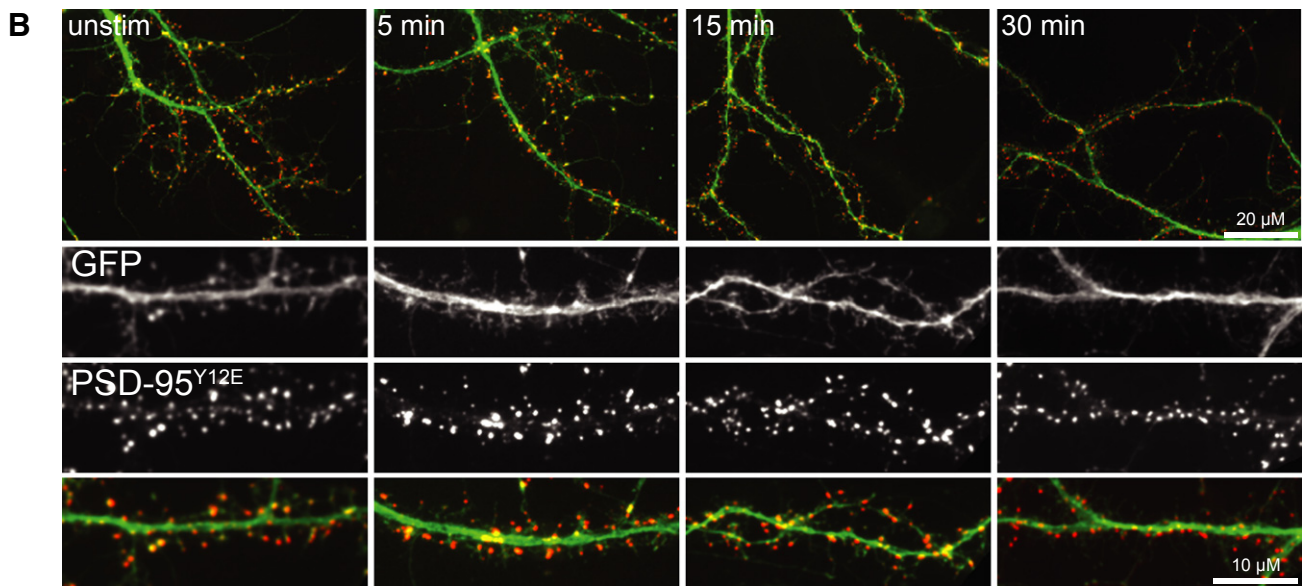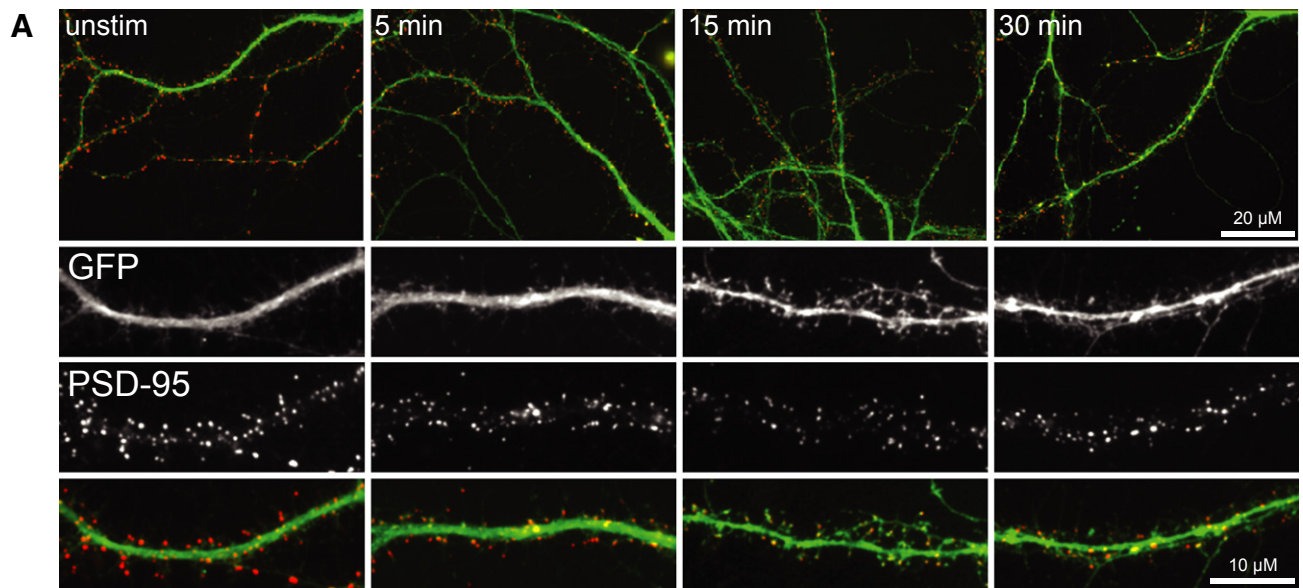
Figure 7. Ca²⁺/CaM binding to the N-terminus of PSD-95 is important for loss of PSD-95 from spines upon Ca²⁺ influx.

A, B   Hippocampal cultures were transfected at 4 DIV with plain GFP as volume marker and PSD-95^{WT} (A) or PSD-95^{Y12E} (B) carrying TagRFP at their C-termini. At 18 DIV, cultures were treated for 2 min with vehicle or glutamate (100 µM) and the NMDA-type glutamate receptor co-agonist glycine (10 µM). Cells were fixed 5, 15, and 30 min after treatment.

C   Co-localized GFP and RFP puncta were normalized to the respective intensity in the dendritic shaft to account for differences in expression levels. Synaptic enrichment was assessed as ratio of RFP to GFP for every synaptic area (assessed by RFP fluorescence). All values were normalized to unstimulated cells. The time courses of the change in synaptic enrichment of PSD-95^{WT} ($t = 0$: 1.00 ± 0.06; $t = 5$: 0.95 ± 0.05; $t = 15$: 0.81 ± 0.07, $*P < 0.05$; $t = 30$: 0.90 ± 0.06; one-way ANOVA with Bonferroni's multiple comparison test) and PSD-95^{Y12E} ($t = 0$: 1.00 ± 0.07; $t = 5$: 1.47 ± 0.09, $**P < 0.01$; $t = 15$: 1.26 ± 0.11; $t = 30$: 0.90 ± 0.11; one-way ANOVA with Bonferroni's multiple comparison test) are significantly different after 5 min (two-way ANOVA, Bonferroni's post-test, $F_{1,265} = 14.62$, $***P < 0.001$) and 15 min ($**P < 0.01$) of washout (values are mean ± s.e.m., $n = 17$–60 cells from four independent experiments).

D   As a proxy for synapse size, the area of individual RFP puncta was compared between PSD-95^{WT} ($t = 0$: 4.51 ± 0.12 µm; $t = 5$: 4.40 ± 0.08; $t = 15$: 4.08 ± 0.11, $*P < 0.05$; $t = 30$: 4.17 ± 0.17; one-way ANOVA with Bonferroni's multiple comparison test) and PSD-95^{Y12E} ($t = 0$: 4.40 ± 0.15 µm; $t = 5$: 4.35 ± 0.08; $t = 15$: 4.17 ± 0.10; $t = 30$: 4.07 ± 0.15).

EGTA, 10 mM Tris-HCl, pH 7.4 and protease inhibitors) before ultracentrifugation.

Immunoprecipitation and immunoblotting

Immunoprecipitation and immunoblotting were performed as in Hell *et al*, 1993. Multiple exposure times ensured that immunosignals were in the linear range (Davare & Hell, 2003; Hall *et al*, 2006). Signals were quantified through densitometry using Photoshop CS3 software (Adobe).

Primary hippocampal neuronal cultures

Cultures were prepared from E18 rat embryos and grown on cover-slips coated with 0.1% (w/v) poly-L-lysine at a cell density of 3×10^4/cm² in Neurobasal medium (Life Technologies) supplemented

with NS21 (Chen *et al*, 2008) as described (Chen *et al*, 2008; Halt *et al*, 2012; Hall *et al*, 2013).

NMR spectroscopy

Proteins were expressed in *E. coli* strain BL21 (DE3) in LB medium (unlabeled proteins) or M9 media supplemented with $^{15}NH_4Cl$ or $^{15}NH_4Cl/^{13}C$-glucose for single- or double-labeled proteins. CaM was prepared as described (Zhang *et al*, 2012). GST- or His-tagged PSD-95(1–71) were purified from *E. coli* supernatants by standard affinity purification on GST columns (Hengen, 1996; Smith, 2000) or Ni-NTA columns (Bornhorst & Falke, 2000). Purified GST-fusion protein was digested by thrombin to remove the N-terminal GST tag, producing an N-terminal fragment of PSD-95 [residues 1–71, called PSD-95(1–71)] that was further purified by gel-filtration size-exclusion chromatography (Superdex 75). PSD-95(1–71) containing
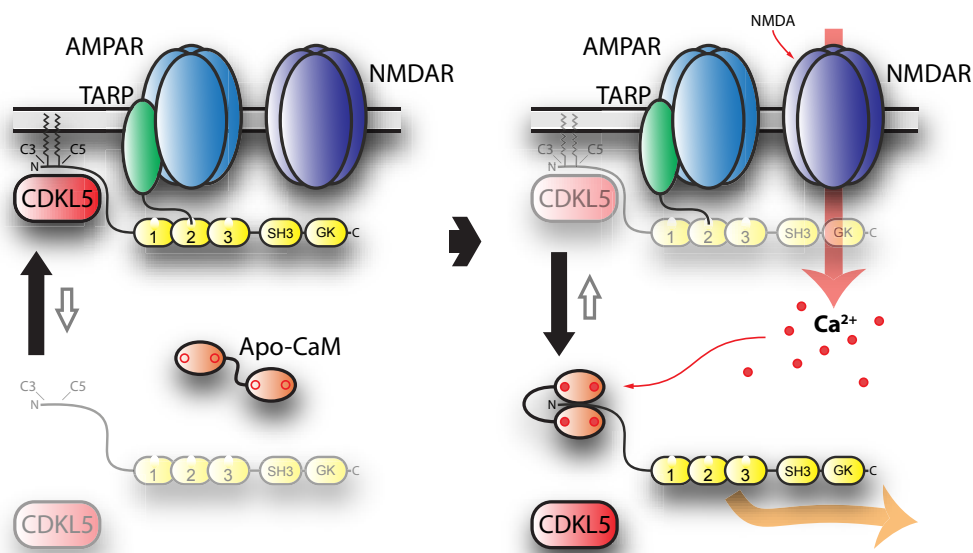
Figure 8. Model of Ca²⁺/CaM-induced postsynaptic release of PSD-95.
(Left) Under basal conditions, PSD-95 (yellow) is attached to the postsynaptic site through palmitoylation of C3 and C5. It keeps AMPA-type glutamate receptors (blue) via binding with its first and second PDZ domains to the C-termini of their auxiliary TARP subunits (green) at postsynaptic sites. It also anchors CDKL5 (red) via its palmitoylated N-terminus. PSD-95 frequently cycles between palmitoylation and depalmitoylation. (Right) Ca²⁺ influx through NMDA-type glutamate receptors induces binding of Ca²⁺/CaM to depalmitoylated PSD-95 to prevent re-palmitoylation. Consequently, a fraction of PSD-95 leaves the postsynaptic site and CDKL5 anchoring is reduced.

a C-terminal His-tag from Ni-NTA column was loaded onto a size-exclusion column (Superdex 75) for further purification.

The purified ^{15}N- or ^{13}C/^{15}N-labeled PSD95(1–71) protein was exchanged into NMR buffer (25 mM CD$_3$COONa, 1 mM EDTA-d, 5 mM DTT-d, 8% D$_2$O, pH5.0). The NMR samples of ^{15}N- or ^{13}C/^{15}N-labeled CaM bound to unlabeled PSD-95(1–71) were prepared by adding 1.5-fold excess of unlabeled PSD95(1–71) to labeled CaM and vice versa. Briefly, the pure CaM and PSD-95(1–71) proteins were separately exchanged into NMR buffer (pH7.0) containing 20 mM Tris-d_{11} with 5 mM CaCl$_2$, 50 mM NaCl, 5 mM DTT-d and 95% H$_2$O/5% D$_2$O. The isotopically labeled Ca^{2+}-bound CaM (0.3 mM) was mixed with an equal volume of PSD-95(1–71) (0.45 mM) and then concentrated to give a final concentration of 0.3 mM for the 1:1 complex (called CaM/PSD95) in a final volume of 0.3 ml.

For the measurement of RDCs of CaM bound to PSD-95(1–71), the filamentous bacteriophage Pf1 (Asla Biotech Ltd., Latvia) was used as an orienting medium. Pf1 (17 mg/ml) was added to ^{15}N-labeled CaM bound to unlabeled PSD-95(1–71) at pH 7.0, to produce weak alignment of the complex.

All NMR experiments were performed with 800 MHz Bruker Avance III spectrometer equipped with TCI cryoprobe. NMR resonance assignments were obtained as described by Zhang *et al*, 2012. ^{15}N $T1$, $T2$, and ^{15}N-{^{1}H} NOE experiments were performed on PSD-95(1–71) at 283K or CaM bound to PSD-95(1–71) at 310K using standard pulse sequences described previously (Farrow *et al*, 1994).

Author contribution

YZ, LM, TP, ZM, DC, AR, JBA, and JWH designed experiments; YZ, LM, TP, ZM, DC, and DKP performed experiments; YZ, LM, TP, ZM, DC, DKP, AR, JBA, and JWH analyzed data; YZ, LM, TP, DC, AR, JBA, and JWH wrote the manuscript.

Conflict of interest

The authors declare that they have no conflict of interest.

References

Bartos JA, Ulrich JD, Li H, Beazely MA, Chen Y, Macdonald JF, Hell JW (2010) Postsynaptic clustering and activation of Pyk2 by PSD-95. *J Neurosci* 30: 449–463

Bornhorst JA, Falke JJ (2000) Purification of proteins using polyhistidine affinity tags. *Methods Enzymol* 326: 245–254

Chen L, Chetkovich DM, Petralia RS, Sweeney NT, Kawasaki Y, Wenthold RJ, Bredt DS, Nicoll RA (2000) Stargazin regulates synaptic targeting of AMPA receptors by two distinct mechanisms. *Nature* 408: 936–943

Chen Y, Stevens B, Chang J, Milbrandt J, Barres BA, Hell JW (2008) xml: re-defined and modified supplement B27 for neuronal cultures. *J Neurosci Methods* 171: 239–247

Davare MA, Hell JW (2003) Increased phosphorylation of the neuronal L-type Ca(^{2}) channel Ca(v)1.2 during aging. *Proc Natl Acad Sci USA* 100: 16018–16023

Dick IE, Tadross MR, Liang H, Tay LH, Yang W, Yue DT (2008) A modular switch for spatial Ca^{2+} selectivity in the calmodulin regulation of CaV channels. *Nature* 451: 830–834

El-Husseini A, Schnell E, Dakoji S, Sweeney N, Zhou Q, Prange O, Gauthier C, Aquilera A, Nicoll RA, Bredt DS (2002) Synaptic strength regulated by palmitate cycling on PSD-95. *Cell* 108: 849–863

El-Husseini AE, Schnell E, Chetkovich DM, Nicoll RA, Bredt DS (2000) PSD-95 involvement in maturation of excitatory synapses. *Science* 290: 1364–1368

Elias GM, Funke L, Stein V, Grant SG, Bredt DS, Nicoll RA (2006) Synapse-specific and developmentally regulated targeting of AMPA receptors by a family of MAGUK scaffolding proteins. *Neuron* 52: 307–320

Evans TI, Hell JW, Shea MA (2011) Thermodynamic linkage between calmodulin domains binding calcium and contiguous sites in the C-terminal tail of Ca(V)1.2. *Biophys Chem* 159: 172–187

Farrow NA, Muhandiram R, Singer AU, Pascal SM, Kay CM, Gish G, Shoelson SE, Pawson T, Kay LE (1994) Backbone dynamics of a free and phosphopeptide-complexed Src homology 2 domain studied by 15N NMR relaxation. *Biochemistry* 33: 5984–6003

Fukata M, Fukata Y, Adesnik H, Nicoll RA, Bredt DS (2004) Identification of PSD-95 palmitoylating enzymes. *Neuron* 44: 987–996

Fukata Y, Dimitrov A, Boncompain G, Vielemeyer O, Perez F, Fukata M (2013) Local palmitoylation cycles define activity-regulated postsynaptic subdomains. *J Cell Biol* 202: 145–161

Fukunaga Y, Matsubara M, Nagai R, Miyazawa A (2005) The interaction between PSD-95 and Ca^{2+}/calmodulin is enhanced by PDZ-binding proteins. *J Biochem* 138: 177–182

Hall DD, Dai S, Tseng PY, Malik Z, Nguyen M, Matt L, Schnizler K, Shephard A, Mohapatra DP, Tsuruta F, Dolmetsch RE, Christel CJ, Lee A, Burette A, Weinberg RJ, Hell JW (2013) Competition between a-actinin and Ca^{2+}-calmodulin controls surface retention of the L-type Ca^{2+} channel Ca(V)1.2. *Neuron* 78: 483–497

Hall DD, Feekes JA, Arachchige AS, Shi M, Hamid J, Chen L, Strack S, Zamponi GW, Horne MC, Hell JW (2006) Binding of protein phosphatase 2A to the L-type calcium channel Cav1.2 next to Ser 1928, its main PKA site, is critical for Ser1928 dephosphorylation. *Biochemistry* 45: 3448–3459

Halt AR, Dallapiazza RF, Zhou Y, Stein IS, Qian H, Juntti S, Wojcik S, Brose N, Silva AJ, Hell JW (2012) CaMKII binding to GluN2B is critical during memory consolidation. *EMBO J* 31: 1203–1216

Hell JW, Westenbroek RE, Warner C, Ahlijanian MK, Prystay W, Gilbert MM, Snutch TP, Catterall WA (1993) Identification and differential subcellular localization of the neuronal class C and class D L-type calcium channel alpha 1 subunits. *J Cell Biol* 123: 949–962

Hengen PN (1996) Methods and reagents: purification of GST fusion proteins. *Trends Biochem Sci* 21: 400–401

Hoeflich KP, Ikura M (2002) Calmodulin in action: diversity in target recognition and activation mechanisms. *Cell* 108: 739–742

Hsueh YP, Sheng M (1999) Requirement of N-terminal cysteines of PSD-95 for PSD-95 multimerization and ternary complex formation, but not for binding to potassium channel Kv1.4. *J Biol Chem* 274: 532–536

Ikura M (1996) Calcium binding and conformational response in EF-hand proteins. *Trends Biochem Sci* 21: 14–17

Johny MB, Yang PS, Bazzazi H, Yue DT (2013) Dynamic switching of calmodulin interactions underlies Ca^{2+} regulation of CaV1.3 channels. *Nat Commun* 4:1717

Kurokawa H, Osawa M, Kurihara H, Katayama N, Tokumitsu H, Swindells MB, Kainosho M, Ikura M (2001) Target-induced conformational adaptation of calmodulin revealed by the crystal structure of a complex with nematode Ca$^{(2+)}$/calmodulin-dependent kinase peptide. *J Mol Biol* 312: 59−68

Leonard AS, Lim IA, Hemsworth DE, Horne MC, Hell JW (1999) Calcium/calmodulin-dependent protein kinase II is associated with the N-methyl-D-aspartate receptor. *Proc Natl Acad Sci USA* 96: 3239−3244

Lim IA, Hall DD, Hell JW (2002) Selectivity and promiscuity of the first and second PDZ domains of PSD-95 and synapse-associated protein 102. *J Biol Chem* 277: 21697−21711

Lisman JE, Hell JW (2008) Long-term potentiation. In *Structural and Functional Organization of the Synapse*, Hell JW, Ehlers MD (eds), pp 501−534. Heidelberg: Springer

Masuko N, Makino K, Kuwahara H, Fukunaga K, Sudo T, Araki N, Yamamoto H, Yamada Y, Miyamoto E, Saya H (1999) Interaction of NE-dlg/SAP102, a neuronal and endocrine tissue-specific membrane-associated guanylate kinase protein, with calmodulin and PSD-95/SAP90. A possible regulatory role in molecular clustering at synaptic sites. *J Biol Chem* 274: 5782−5790

Micheva KD, Busse B, Wiler NC, O'Rourke N, Smith SJ (2010) Single-synapse analysis of a diverse synapse population: proteomic imaging methods and markers. *Neuron* 68: 639−653

Morris RG (2013) NMDA receptors and memory encoding. *Neuropharmacol* 74: 32−40

Nelson CD, Kim MJ, Hsin H, Chen Y, Sheng M (2013) Phosphorylation of threonine-19 of PSD-95 by GSK-3ß is required for PSD-95 mobilization and long-term depression. *J Neurosci* 33: 12122−12135

Nicoll RA, Roche KW (2013) Long-term potentiation: peeling the onion. *Neuropharmacol* 74: 18−22

Opazo P, Labrecque S, Tigaret CM, Frouin A, Wiseman PW, De Koninck P, Choquet D (2010) CaMKII triggers the diffusional trapping of surface AMPARs through phosphorylation of stargazin. *Neuron* 67: 239−252

Paarmann I, Spangenberg O, Lavie A, Konrad M (2002) Formation of complexes between Ca^{2+} calmodulin and the synapse-associated protein SAP97 requires the SH3 domain-guanylate kinase domain-connecting HOOK region. *J Biol Chem* 277: 40832−40838

Pitt GS, Zuhlke RD, Hudmon A, Schulman H, Reuter H, Tsien RW (2001) Molecular basis of calmodulin tethering and Ca^{2+}-dependent inactivation of L-type Ca^{2+} channels. *J Biol Chem* 276: 30794−30802

Rhoads AR, Friedberg F (1997) Sequence motifs for calmodulin recognition. *FASEB J* 11: 331−340

Ricciardi S, Ungaro F, Hambrock M, Rademacher N, Stefanelli G, Brambilla D, Sessa A, Magagnotti C, Bachi A, Giarda E, Verpelli C, Kilstrup C, Sala C, Kalscheuer VM, Broccoli V (2012) CDKL5 ensures excitatory synapse stability by reinforcing NGL-1-PSD95 interaction in the postsynaptic compartment and is impaired in patient iPSC-derived neurons. *Nat Cell Bio* 14: 911−923

Schluter OM, Xu W, Malenka RC (2006) Alternative N-terminal domains of PSD-95 and SAP97 govern activity-dependent regulation of synaptic AMPA receptor function. *Neuron* 51: 99−111

Schnell E, Sizemore M, Karimzadegan S, Chen L, Bredt DS, Nicoll RA (2002) Direct interactions between PSD-95 and stargazin control synaptic AMPA receptor number. *Proc Natl Acad Sci USA* 99: 13902−13907

Smith DB (2000) Generating fusions to glutathione S-transferase for protein studies. *Methods Enzymol* 326: 254−270

Steiner P, Higley MJ, Xu W, Czervionke BL, Malenka RC, Sabatini BL (2008) Destabilization of the postsynaptic density by PSD-95 serine 73 phosphorylation inhibits spine growth and synaptic plasticity. *Neuron* 60: 788−802

Sturgill JF, Steiner P, Czervionke BL, Sabatini BL (2009) Distinct domains within PSD-95 mediate synaptic incorporation, stabilization, and activity-dependent trafficking. *J Neurosci* 29: 12845−12854

Sumioka A, Yan D, Tomita S (2010) TARP phosphorylation regulates synaptic AMPA receptors through lipid bilayers. *Neuron* 66: 755−767

Tjandra N, Bax A (1997) Direct measurement of distances and angles in biomolecules by NMR in a dilute liquid crystalline medium. *Science* 278: 1111−1114

Tomita S, Stein V, Stocker TJ, Nicoll RA, Bredt DS (2005) Bidirectional synaptic plasticity regulated by phosphorylation of stargazin-like TARPs. *Neuron* 45: 269−277

Vartak N, Papke B, Grecco HE, Rossmannek L, Waldmann H, Hedberg C, Bastiaens PI (2014) The autodepalmitoylating activity of APT maintains the spatial organization of palmitoylated membrane proteins. *Biophys J* 106: 93−105

de Vries SJ, van Dijk M, Bonvin AM (2010) The HADDOCK web server for data-driven biomolecular docking. *Nat Protoc* 5: 883−897

Zhang Y, Li Z, Sacks DB, Ames JB (2012) Structural basis for Ca^{2+}-induced activation and dimerization of estrogen receptor a by calmodulin. *J Biol Chem* 287: 9336−9344

Zhu Y, Li D, Wang L, Lu B, Zheng J, Zhao S, Zeng R, Xiong Z (2013) Palmitoylation-dependent CDKL5−PSD-95 interaction regulates synaptic targeting of CDKL5 and dendritic spine development. *Proc Natl Acad Sci USA* 110: 9118−9123